

Dust impact voltage signatures on Parker Solar Probe: influence of spacecraft floating potential

S. D. Bale^{1,2}, K. Goetz³, J. W. Bonnell¹, A. W. Case⁴, C. H. K. Chen⁵, T. Dudok de Wit⁶,
L. C. Gasque^{1,2}, P. R. Harvey¹, J. C. Kasper^{7,4}, P. J. Kellogg³, R. J. MacDowall⁸, M.
Maksimovic⁹, D. M. Malaspina¹⁰, B. F. Page^{1,2}, M. Pulupa¹, M. L. Stevens⁴, J. R.
Szalay¹¹, A. Zaslavsky⁹

¹Space Sciences Laboratory, University of California, Berkeley, CA 94720-7450, USA

²Physics Department, University of California, Berkeley, CA 94720-7300, USA

³School of Physics and Astronomy, University of Minnesota, Minneapolis, 55455, USA

⁴Smithsonian Astrophysical Observatory, Cambridge, MA 02138 USA

⁵School of Physics and Astronomy, Queen Mary University of London, London E1 4NS, UK

⁶LPC2E, CNRS and University of Orléans, Orléans, France

⁷Climate and Space Sciences and Engineering, University of Michigan, Ann Arbor, MI 48109, USA

⁸Solar System Exploration Division, NASA/Goddard Space Flight Center, Greenbelt, MD, 20771

⁹LESIA, Observatoire de Paris, Université PSL, CNRS, Sorbonne Université, Université de Paris, 5 place Jules

Janssen, 92195 Meudon, France

¹⁰Laboratory for Atmospheric and Space Physics, University of Colorado, Boulder, CO, 80303, USA

¹¹Department of Astrophysical Sciences, Princeton University, Princeton, NJ, 08544, USA

Key Points:

- The Parker Solar Probe (PSP) FIELDS instrument measures millisecond voltages impulses associated with dust impacts
- The sign of the largest monopole voltage response is a function of the spacecraft floating potential
- These measurements are consistent with models of dynamic charge balance following dust impacts

Submitted : June 2, 2020

Abstract

When a fast dust particle hits a spacecraft, it generates a cloud of plasma some of which escapes into space and the momentary charge imbalance perturbs the spacecraft voltage with respect to the plasma. Electrons race ahead of ions, however both respond to the DC electric field of the spacecraft. If the spacecraft potential is positive with respect to the plasma, it should attract the dust cloud electrons and repel the ions, and vice versa. Here we use measurements of impulsive voltage signals from dust impacts on the Parker Solar Probe (PSP) spacecraft to show that the peak voltage amplitude is clearly related to the spacecraft floating potential, consistent with theoretical models and laboratory measurements. In addition, we examine some timescales associated with the voltage waveforms and compare to the timescales of spacecraft charging physics.

Plain Language Summary

When a fast, interplanetary dust particle hits a spacecraft, it generates a shock in the spacecraft material that liberates a hot, ionized plasma. Some of the plasma ions and electrons return immediately to the spacecraft, but some escape into space. The momentary charge imbalance created by the different ion and electron speeds generates a transient perturbation to the voltage of the spacecraft. However, these electrons and ions can be attracted or repelled depending on the DC electric field of the spacecraft itself. In this paper, we show this effect clearly: when the spacecraft floating voltage is negative with respect to the interplanetary plasma, the electrons from the dust impact are repelled and vice-versa.

1 Voltage signatures of dust impacts on spacecraft

Plasma wave electric field measurements in space have proven to be powerful diagnostic of planetary (Scarf et al., 1983; Gurnett et al., 1987; Meyer-Vernet et al., 2009; Ye et al., 2014) and interplanetary (Gurnett et al., 1997; Zaslavsky et al., 2012; Malaspina et al., 2014; Kellogg et al., 2016) dust processes. A hypervelocity dust impact onto the spacecraft body or antenna produces a plasma cloud and the momentary charge imbalance generates a rapid perturbation to the spacecraft floating potential. Some of the resulting plasma is recaptured by the spacecraft and some of it escapes, depending on the energy of the ions and electrons and the spacecraft-to-plasma electric potential. Monopole (probe-to-spacecraft) or dipole (probe-to-probe) voltage measurements will record millisecond-timescale spikes and/or their spectral content. These effects have been explored in several recent papers (Zaslavsky, 2015; Vaverka et al., 2017; Kellogg et al., 2018; Vaverka et al., 2019; Kellogg et al., 2020) and recently reviewed by Mann et al. (2019).

During the first PSP solar encounters, PSP/FIELDS measurements of dust impact rates were used to map the radial variation the flux of the interplanetary dust. Page et al. (2020) used dipole voltage signals to infer the dust velocity vector and comparison with models (Szalay et al., 2020) suggests that this dust population is consistent with β micrometeoroids on exiting hyperbolic orbits. Malaspina et al. (2020) compared data from Encounters 1-3 to show that the population is variable and probably has its source between 10-30 R_S . While the PSP/WISPR instrument saw the beginnings of a decrease in F corona intensity (Howard et al., 2019).

Here we examine the sign of the monopole antenna measurements from the PSP/FIELDS instrument; these observations show that the spacecraft voltage perturbation is influenced by the initial spacecraft potential itself. If the spacecraft is initially negatively charged, it will attract more ions and repel more electrons from the plasma cloud producing a large positive perturbation. If initially positively charged, the op-

posite occurs and returning electrons produce a large negative polarity spike. We also examine some typical timescales associated with these perturbations and suggest that they are associated with the escape process.

2 Parker Solar Probe Measurements

The Parker Solar Probe (PSP) mission (Fox et al., 2016) was launched in August 2018 into an orbit that will take it deep into the inner heliosphere with a final perihelion distance of $9.8 R_S$ from the center of the Sun. This study uses measurements from the PSP/FIELDS (Bale et al., 2016) and the PSP/SWEAP (Kasper et al., 2016) instruments primarily from PSP Encounter 2, between March 23, 2019 and April 13, 2020 to investigate the role of the spacecraft floating (DC) voltage on the voltage signature of dust impacts onto the spacecraft. Perihelion of Encounter 2 was on April 5, 2019 at ≈ 35.7 solar radii (R_S).

Our primary measurements are made by the Time Domain Sampler (TDS) subsystem of the PSP/FIELDS instrument (Bale et al., 2016). The TDS makes rapid samples of waveforms with simultaneous sampling of five analog channels which can be selected from dipole antennas pairs, monopoles, or a high-frequency search coil magnetometer (Bale et al., 2016). During PSP Encounters 2 and 3 (used here), the TDS was configured to sample at 1.92 MSa/s and produce 32768-point waveform ‘events’; therefore each TDS event is 17.067 ms in duration. In addition to the TDS waveform events, the TDS records a ‘TDS Max’ value each 7 seconds during nominal encounter mode. The TDS Max value is the signed extreme of the entire datastream during the interval and is dominated by the large voltage signatures of dust impacts.

We use TDS measurements of the voltage between the ‘V2’ monopole antenna and spacecraft ground V_G and we call this measurement $\delta V_2 = V_2 - V_G$. The δ emphasizes the fact that the TDS measurement is band-pass filtered (i.e. *not* DC-coupled); the TDS system has a flat gain and phase response from 1 kHz to 1 MHz (1 ms - 1 μ s) and the waveforms shown here have not been corrected with a transfer function, which will not change our results on these timescales. The measurement represents the voltage perturbation between the probe-spacecraft system. Note that a positive perturbation of the spacecraft ground/potential at a fixed probe potential is measured as a negative voltage impulse in δV_2 . The V2 monopole is mounted near the plane of the spacecraft heatshield at $-\cos(55^\circ)\hat{x} - \sin(55^\circ)\hat{y}$ in the spacecraft coordinate system. During PSP solar encounter, the spacecraft \hat{x} axis points southward and the \hat{y} axis points approximately in the ram direction, therefore the V2 monopole is on the anti-ram side during the normal solar encounter configuration (Bale et al., 2016). The PSP/FIELDS electric antennas are 2m long, 1/8” diameter thin-walled tubes of C103 Niobium alloy and have a free space capacitance of $C_A \sim 18$ pF and a system stray (base) capacitance of $C_B \sim 26$ pF (Pulupa et al., 2017). The (post-anneal) photoelectron threshold of C103 Niobium is $E_{103} \sim 4.72$ eV (Diaz-Aguado et al., 2019) and we assume a photoelectron temperature of $T_{ph} \sim 1.5$ eV.

For PSP Encounters 1 and 2, TDS was programmed to capture waveforms with the largest absolute amplitude and that algorithm returned predominantly dust impact events. For Encounter 3, a new algorithm was implemented that favors a combination of large amplitude *and* a large number of zero-crossings. This algorithm generated primarily plasma wave events during Encounter 3. Figure 1 is a histogram of both minimum and maximum amplitude from 511 waveform events on September 1, 2019 of Encounter 3 near perihelion. All of these events are plasma waves, as identified by eye, and it can be seen that none exceed ± 25 mV amplitude. We therefore choose ± 25 mV as our threshold beyond which we consider our measurements to be dust impacts, rather than plasma waves. Page et al. (2020) used a threshold of 50 mV, which produces qualitatively similar results for this analysis, but fewer counts.

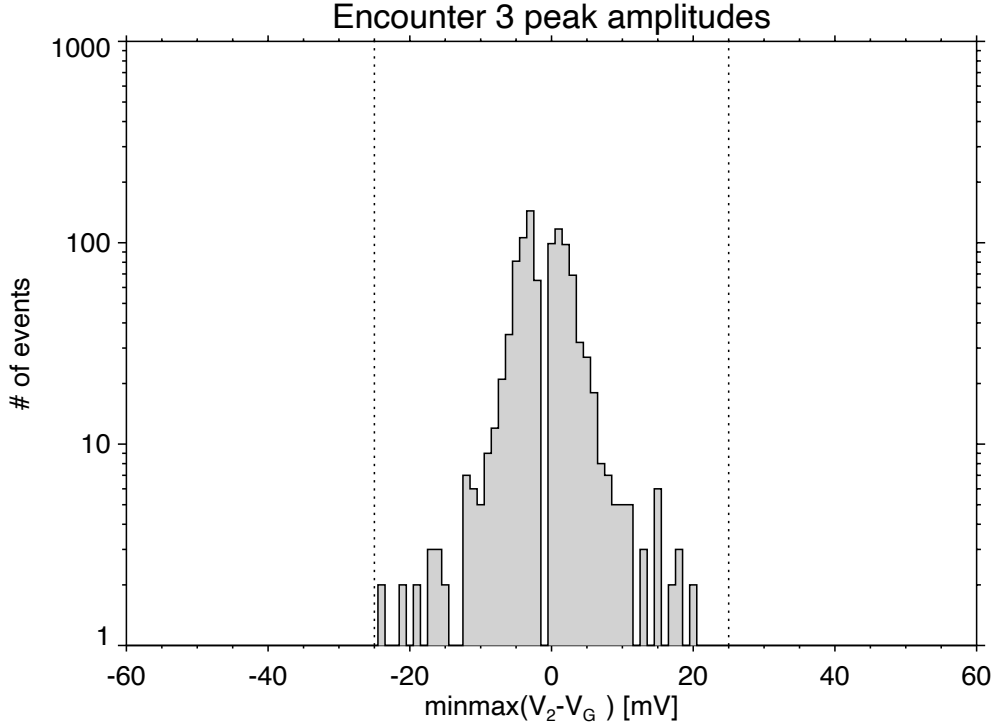


Figure 1. Histogram of minimum and maximum waveform amplitudes on the V_2 monopole during Encounter 3 on September 1, 2019 ($R < 36 R_S$), comprising 511 waveform events each represented here with a maximum and minimum data value. Encounter 3 uses a burst waveform selection algorithm that selects plasma waves, rather than dust impacts. The measurements here represent a mix of ion acoustic, electrostatic whistler, and Langmuir waves. Dotted vertical lines at ± 25 mV are our threshold for dust events during Encounter 2.

Our ‘spacecraft potential’ measurement V_{SC} is computed as the negative of the average DC-coupled voltage on all four monopole antennas $V_{SC} = -(V_1 + V_2 + V_3 + V_4)/4$ from the Digital Fields Board (DFB) subsystem (Malaspina et al., 2016). The voltage probes V_i are current-biased to hold them near the local plasma potential, therefore this quantity should represent the floating potential of the spacecraft (Pedersen, 1995; Guillemant et al., 2012). However it is important to note that the PSP heatshield on the sunward side of the spacecraft is *not* directly electrically connected to the spacecraft body itself; electrical coupling between the heatshield and spacecraft body is carried by plasma and body currents only. Therefore this measured V_{SC} may not represent the true floating potential of the entire heatshield-spacecraft system. Furthermore, modeling has suggested that for very high photoelectron densities, space-charge effects may produce a double layer at the sunward surface of the heatshield and a plasma wake behind that may modify its floating potential (Ergun et al., 2010; Guillemant et al., 2012). Note that we differentiate V_{SC} from V_G ; V_{SC} is the DC-coupled spacecraft potential measured by the DFB, while V_G is the spacecraft potential reference for the TDS band-passed δV_2 measurement.

We also use electron (total plasma) density and electron core temperature measurements produced from an analysis of the quasi-thermal noise spectrum (Meyer-Vernet & Perche, 1989) during PSP Encounter 2. This technique was also applied to Encounter 1 data and described in Moncuquet et al. (2020). Ion temperature mea-

measurements are derived from SWEAP instrument moment calculations of the total ion distribution from the Solar Probe Cup instrument (Kasper et al., 2016; Case et al., 2020).

3 Results

Figure 2 shows an overview of PSP Encounter 2 measurements from March 27 to April 13, 2019. The top panel [a] is the total plasma density n_e measured from the plasma frequency peaks in the quasi-thermal noise spectrum (Meyer-Vernet & Perche, 1989; Moncuquet et al., 2020). The density reaches a peak value of around $n_e \sim 600 \text{ cm}^{-3}$ on April 3 at $r \sim 39 R_S$. Panel [b] is the spacecraft potential V_{SC} as described in Section 2 above, colored for polarity (red > 0 , blue < 0), the values range between -4 and +4 Volts. Note that higher plasma density intervals correspond to more negative spacecraft floating potential, as expected (Pedersen, 1995). Panel [c] shows the number of dust events in 30 minute intervals, assuming that TDS Max values of $|V_2| > 25 \text{ mV}$ are attributable to a dust impact and shows the trend of increasing dust impacts with radial distance as shown previously (Page et al., 2020; Malaspina et al., 2020; Szalay et al., 2020). Panel [d] is the number of positive polarity dust events ($V_2 > 25 \text{ mV}$) per 30 minutes, with red dots indicating intervals of positive V_{SC} from panel [b] and panel [e] is the number of negative polarity dust events ($V_2 < -25 \text{ mV}$) with blue dots indicating intervals of negative spacecraft potential. The bottom panel [f] shows the bias current applied to the V2 antenna, indicating an interval of no bias, as well as times when the fixed bias was disabled during bias current calibration sweeps. The sweep intervals were deleted from the statistics to keep the sweeps from contaminating the dust impact measurements.

The striking feature of Figure 2 is the relationship between the sign of the spacecraft potential in panel [b] and the sign of the dust voltage impact signal in panels [d] and [e]; negative polarity spacecraft potential tends to produce negative impulse TDS events $\delta V_2 = V_2 - V_G$, i.e. positive perturbations to V_G assuming a fixed V_2 . This is consistent with the idea that a negatively charged spacecraft $V_{SC} < 0$ repels the dust cloud electrons producing a positive voltage perturbation δV_G (therefore a negative perturbation to $\delta V_2 = V_2 - V_G$), and vice-versa. Note that this behavior is consistent with plasma cloud ions and electrons having temperatures on the order of $\sim 1 \text{ V}$, as described further below.

Note also that in some cases of high density (panel [a]) and therefore negative V_{SC} (panel [b]), there appears to be enhanced overall count levels (panel [c]), suggesting that the spacecraft floating voltage may influence or modify the overall dust impact rate by perhaps providing a threshold for the measured charge.

This effect can also be seen by examining the waveforms themselves; we use waveforms from April 3, 2019, the interval between green vertical bars in Figure 2. Figure 3 shows superposed-epoch averaged waveforms, with 1σ deviations, and organized by intervals of spacecraft potential V_{SC} . The number of waveforms used to compute the average and variance in each row is given in column 2 of Table 1. Each individual waveform is shifted to start at $t=0$ by finding the initial perturbation above $5 * V_{noise}$, where V_{noise} is the RMS level of the first 4 ms of the waveform (before the dust signal). This level is typically $V_{noise} \approx 0.5 \text{ mV}$. While there is considerable variability between the waveforms, they generally exhibit some common features: an initial rapid negative excursion, a peak at $T \lesssim 0.1 \text{ ms}$, and another peak at $0.2 \lesssim T \lesssim 0.5 \text{ ms}$. The voltage impulse settles back to V_{noise} at times $T \gtrsim 2 \text{ ms}$. The average waveforms are plotted together in Figure 4 and colored for range of V_{SC} , with several timescales annotated and collected in Table 1.

Table 1. Parameters associated with TDS epoch-averaged waveforms in Figure 4 and plasma parameters as described in the text.

V_{SC} [V]	#	$\langle n_e \rangle$ [cm^{-3}]	$\langle T_e \rangle$ [eV]	$\langle T_i \rangle$ [eV]	$\langle \tau_{pe} \rangle$ [ms]	$\langle \tau_{ce} \rangle$ [ms]	$\langle \tau_{SC} \rangle$ [ms]	T_1 [ms] 1st z/c	T_2 [ms] 2nd peak	T_3 [ms] 2nd z/c	T_4 [ms] 3rd peak	T_5 [ms] $\rightarrow V_{noise}$
(-2.5, -1.5)	19	571	25	9	0.005	0.436	0.244	-	0.037	0.310	0.463	3.346
(-1.5, -0.5)	31	515	25	10	0.005	0.448	0.256	0.013	0.076	0.176	0.286	4.208
(-0.5, 0.5)	19	352	32	13	0.006	0.403	0.421	0.002	0.066	0.165	0.266	3.532
(0.5, 1.5)	57	177	28	11	0.008	0.369	0.797	0.006	0.061	0.192	0.294	2.786
(1.5, 2.5)	84	163	30	11	0.009	0.366	0.927	0.006	0.043	0.175	0.288	2.395

The columns in Table 1 list (left-to-right) the interval of V_{SC} in Volts, the number of waveform events in that interval, the average plasma density $\langle n_e \rangle$, electron core temperature $\langle T_e \rangle$, ion temperature $\langle T_i \rangle$, the electron plasma period $\langle \tau_{pe} \rangle$, electron cyclotron period $\langle \tau_{ce} \rangle$, the spacecraft RC time $\langle \tau_{SC} \rangle$ and timescales associated with the 1st zero-crossing, 2nd peak, 2nd zero-crossing, 3rd peak, and relaxation to V_{noise} (zero) respectively, as annotated in Figure 4. In addition, all waveforms with $V_{SC} > -1.5V$ show a small (negative) 1st peak at $T \approx T_1/2$, although these values start to approach the granularity of the measurement $1/(1.92 \text{ MSa/s}) \sim 0.53 \mu\text{s}$. The antenna RC charging time can be estimated as $\tau_A \simeq (C_A T_{ph})/I_{bias}$, which takes values of 0.01 to 0.04 ms during Encounter 2 and is generally less than the spacecraft RC charging time $\tau_{SC} \simeq (C_{SC} T_e)/(A_{SC} n_e e v_{th,e})$ column 8 in Table 1. We estimate C_{SC} as the free space capacitance of a 1m radius sphere $C_{SC} \approx 110 \text{ pF}$. Note that we use the thermal electron temperature to estimate τ_{SC} , rather than the photoelectron temperature (Zaslavsky, 2015) since the spacecraft body is not illuminated; using T_{ph} would result in smaller values of τ_{SC} by a factor of ~ 10 .

Models of dust waveform signatures associate characteristic timescales with the ion and electron collection and escape processes (Zaslavsky, 2015; Meyer-Vernet et al., 2017; Kellogg et al., 2020; Shen, 2020). In particular, escape timescales $\tau_e \sim R_{SC}/v_e$ and $\tau_i \sim R_{SC}/v_i$ can be estimated (Shen, 2020) using impact cloud electron and ion temperatures v_e and v_i (Collette et al., 2016), where $R_{SC} \sim 1\text{m}$ is the spacecraft scale size. If we assign the values of our first peak $T_1/2$ with an electron timescale R_{SC}/v_e and our second peak T_2 with an ion timescale R_{SC}/v_i we find escape speeds of $v_e \approx 150\text{-}1000 \text{ km/s}$ ($\sim 0.3\text{-}3 \text{ eV}$) and $v_i \approx 15\text{-}30 \text{ km/s}$ ($\sim 1\text{-}5 \text{ eV}$, assuming protons). These energies are consistent with laboratory measurements of dust cloud plasma temperatures (Collette et al., 2016). Again, note that there is little or no peak at $T_1/2$ for the waveform with $V_{SC} < -1.5V$ (the most negative values). Note that the timescales associated with the dust impacts arise from charging interactions between the electrons, ions, and the spacecraft, which will be convolved to produce the probe-spacecraft voltage impulse. Our analysis here is very simple and only to suggest that there are multiple timescales evident in the measurement and they can be associated with electron and ion motion. The voltage amplitudes of the waveforms are also interesting and presumably related to the charge generated during impact and the fractions collected and repelled.

4 Conclusions

We show that the sign of the voltage waveforms and onboard voltage extrema are influenced by the DC spacecraft floating potential in a way that is consistent with models of dust plasma cloud dynamics. Timescales associated with the waveforms are broadly consistent with expectations for electron and ion escape energies, and those in turn are at appropriate energies to be influenced by the $\mathcal{O}(\pm 2V)$ spacecraft

potential measurement. As noted above, the measured V_{SC} may not represent the true floating potential of entire spacecraft-heatshield system; as our models of dust plasma cloud escape become more sophisticated, these waveforms may add insight to the actual floating potential of the PSP spacecraft-heatshield system.

More detailed, and statistical, analysis of the PSP/FIELDS dust data is likely to add insight to the physics of dust plasma cloud dynamics, and well as the global distribution of interplanetary dust.

Acknowledgments

The FIELDS experiment on the Parker Solar Probe spacecraft was designed and developed under NASA contract NNN06AA01C. The PSP/FIELDS team acknowledges the extraordinary contributions of the Parker Solar Probe mission operations and spacecraft engineering teams at the Johns Hopkins University Applied Physics Laboratory. SDB acknowledges the support of the Leverhulme Trust Visiting Professorship program. Data access and processing was done using the SPEDAS IDL environment (Angelopoulos et al., 2019). PSP/FIELDS data is publicly available at <http://fields.ssl.berkeley.edu/data/>.

References

- Angelopoulos, V., Cruce, P., Drozdov, A., Grimes, E. W., Hatzigeorgiu, N., King, D. A., ... Schroeder, P. (2019, January). The Space Physics Environment Data Analysis System (SPEDAS). *Space Science Rev.*, 215(1), 9. doi: 10.1007/s11214-018-0576-4
- Bale, S. D., Goetz, K., Harvey, P. R., Turin, P., Bonnell, J. W., Dudok de Wit, T., ... Wygant, J. R. (2016, December). The FIELDS Instrument Suite for Solar Probe Plus. Measuring the Coronal Plasma and Magnetic Field, Plasma Waves and Turbulence, and Radio Signatures of Solar Transients. *Space Science Rev.*, 204(1-4), 49-82. doi: 10.1007/s11214-016-0244-5
- Case, A. W., Kasper, J. C., Stevens, M. L., Korreck, K. E., Paulson, K., Daigneau, P., ... Martinović, M. M. (2020, February). The Solar Probe Cup on the Parker Solar Probe. *Astrophys. J. Suppl.*, 246(2), 43. doi: 10.3847/1538-4365/ab5a7b
- Collette, A., Malaspina, D. M., & Sternovsky, Z. (2016, September). Characteristic temperatures of hypervelocity dust impact plasmas. *Journal of Geophysical Research (Space Physics)*, 121(9), 8182-8187. doi: 10.1002/2015JA022220
- Diaz-Aguado, M. F., Bonnell, J. W., Bale, S. D., Rezvani, S. J., Koshmak, K., Giglia, A., ... Gruntman, M. (2019, January). Experimental Investigation of Total Photoemission Yield from New Satellite Surface Materials. *Journal of Spacecraft and Rockets*, 56(1), 248-258. doi: 10.2514/1.A34245
- Ergun, R. E., Malaspina, D. M., Bale, S. D., McFadden, J. P., Larson, D. E., Mozer, F. S., ... Wygant, J. R. (2010, July). Spacecraft charging and ion wake formation in the near-Sun environment. *Physics of Plasmas*, 17(7), 072903. doi: 10.1063/1.3457484
- Fox, N. J., Velli, M. C., Bale, S. D., Decker, R., Driesman, A., Howard, R. A., ... Szabo, A. (2016, December). The Solar Probe Plus Mission: Humanity's First Visit to Our Star. *Space Science Rev.*, 204(1-4), 7-48. doi: 10.1007/s11214-015-0211-6
- Guillemant, S., Génot, V., Matéo-Vélez, J. C., Ergun, R., & Louarn, P. (2012, July). Solar wind plasma interaction with solar probe plus spacecraft. *Annales Geophysicae*, 30(7), 1075-1092. doi: 10.5194/angeo-30-1075-2012
- Gurnett, D. A., Ansher, J. A., Kurth, W. S., & Granroth, L. J. (1997, January). Micron-sized dust particles detected in the outer solar system by the Voyager 1 and 2 plasma wave instruments. *Geophys. Res. Lett.*, 24(24), 3125-3128. doi: 10.1029/97GL03228
- Gurnett, D. A., Kurth, W. S., Scarf, F. L., Burns, J. A., Cuzzi, J. N., & Grün, E. (1987, December). Micron-sized particle impacts detected near Uranus by the Voyager 2 plasma wave instrument. *Journal of Geophysical Research*, 92(A13), 14959-14968. doi: 10.1029/JA092iA13p14959
- Howard, R. A., Vourlidas, A., Bothmer, V., Colaninno, R. C., DeForest, C. E., Gallagher, B., ... Viall, N. M. (2019, December). Near-Sun observations of an F-corona decrease and K-corona fine structure. *Nature*, 576(7786), 232-236. doi: 10.1038/s41586-019-1807-x
- Kasper, J. C., Abiad, R., Austin, G., Balat-Pichelin, M., Bale, S. D., Belcher, J. W., ... Zank, G. (2016, December). Solar Wind Electrons Alphas and Protons (SWEAP) Investigation: Design of the Solar Wind and Coronal Plasma Instrument Suite for Solar Probe Plus. *Space Science Rev.*, 204(1-4), 131-186. doi: 10.1007/s11214-015-0206-3
- Kellogg, P. J., Goetz, K., & Bale, S. D. (2020). Toward a Physics Based Model of Hypervelocity Dust Impacts. *submitted to Journal of Geophysical Research (Space Physics)*.
- Kellogg, P. J., Goetz, K., & Monson, S. J. (2016, February). Dust impact signals on the wind spacecraft. *Journal of Geophysical Research (Space Physics)*, 121(2), 966-991. doi: 10.1002/2015JA021124
- Kellogg, P. J., Goetz, K., & Monson, S. J. (2018, May). Sign of the Dust Impact-

- Antenna Coupling Cloud. *Journal of Geophysical Research (Space Physics)*, 123(5), 3273-3276. doi: 10.1029/2017JA025173
- Malaspina, D. M., Ergun, R. E., Bolton, M., Kien, M., Summers, D., Stevens, K., ... Goetz, K. (2016, June). The Digital Fields Board for the FIELDS instrument suite on the Solar Probe Plus mission: Analog and digital signal processing. *Journal of Geophysical Research (Space Physics)*, 121(6), 5088-5096. doi: 10.1002/2016JA022344
- Malaspina, D. M., Horányi, M., Zaslavsky, A., Goetz, K., Wilson, L. B., & Kersten, K. (2014, January). Interplanetary and interstellar dust observed by the Wind/WAVES electric field instrument. *Geophys. Res. Lett.*, 41(2), 266-272. doi: 10.1002/2013GL058786
- Malaspina, D. M., Szalay, J. R., Pokorný, P., Page, B., Bale, S. D., Bonnell, J. W., ... Pulupa, M. (2020, April). In Situ Observations of Interplanetary Dust Variability in the Inner Heliosphere. *Astrophys. J.*, 892(2), 115. doi: 10.3847/1538-4357/ab799b
- Mann, I., Nouzák, L., Vaverka, J., Antonsen, T., Fredriksen, Å., Issautier, K., ... Zaslavsky, A. (2019, December). Dust observations with antenna measurements and its prospects for observations with Parker Solar Probe and Solar Orbiter. *Annales Geophysicae*, 37(6), 1121-1140. doi: 10.5194/angeo-37-1121-2019
- Meyer-Vernet, N., Lecacheux, A., Kaiser, M. L., & Gurnett, D. A. (2009, February). Detecting nanoparticles at radio frequencies: Jovian dust stream impacts on Cassini/RPWS. *Geophys. Res. Lett.*, 36(3), L03103. doi: 10.1029/2008GL036752
- Meyer-Vernet, N., Moncuquet, M., Issautier, K., & Schippers, P. (2017, January). Frequency range of dust detection in space with radio and plasma wave receivers: Theory and application to interplanetary nanodust impacts on Cassini. *Journal of Geophysical Research (Space Physics)*, 122(1), 8-22. doi: 10.1002/2016JA023081
- Meyer-Vernet, N., & Perche, C. (1989, March). Tool kit for antennae and thermal noise near the plasma frequency. *J. Geophys. Res.*, 94, 2405-2415. doi: 10.1029/JA094iA03p02405
- Moncuquet, M., Meyer-Vernet, N., Issautier, K., Pulupa, M., Bonnell, J. W., Bale, S. D., ... Malaspina, D. M. (2020, February). First In Situ Measurements of Electron Density and Temperature from Quasi-thermal Noise Spectroscopy with Parker Solar Probe/FIELDS. *Astrophys. J. Suppl.*, 246(2), 44. doi: 10.3847/1538-4365/ab5a84
- Page, B., Bale, S. D., Bonnell, J. W., Goetz, K., Goodrich, K., Harvey, P. R., ... Szalay, J. R. (2020, February). Examining Dust Directionality with the Parker Solar Probe FIELDS Instrument. *Astrophys. J. Suppl.*, 246(2), 51. doi: 10.3847/1538-4365/ab5f6a
- Pedersen, A. (1995, February). Solar wind and magnetosphere plasma diagnostics by spacecraft electrostatic potential measurements. *Annales Geophysicae*, 13(2), 118-129. doi: 10.1007/s00585-995-0118-8
- Pulupa, M., Bale, S. D., Bonnell, J. W., Bowen, T. A., Carruth, N., Goetz, K., ... Sundkvist, D. (2017, March). The Solar Probe Plus Radio Frequency Spectrometer: Measurement requirements, analog design, and digital signal processing. *Journal of Geophysical Research (Space Physics)*, 122(3), 2836-2854. doi: 10.1002/2016JA023345
- Scarf, F. L., Gurnett, D. A., Kurth, W. S., & Poynter, R. L. (1983, January). Voyager plasma wave measurements at Saturn. *Journal of Geophysical Research*, 88(A11), 8637-8638.
- Shen, M. H. e. a. (2020). Antenna signals generated by dust impacts on spacecraft. *submitted to Journal of Geophysical Research (Space Physics)*.
- Szalay, J. R., Pokorný, P., Bale, S. D., Christian, E. R., Goetz, K., Goodrich, K., ... Schwadron, N. (2020, February). The Near-Sun Dust Environment: Initial Observations from Parker Solar Probe. *Astrophys. J. Suppl.*, 246(2), 27. doi: 10.3847/1538-4365/ab50c1

- Vaverka, J., Pavlů, J., Nouzák, L., Šafránková, J., Němeček, Z., Mann, I., ... Lindqvist, P.-A. (2019, November). One-Year Analysis of Dust Impact-Like Events Onto the MMS Spacecraft. *Journal of Geophysical Research (Space Physics)*, 124(11), 8179-8190. doi: 10.1029/2019JA027035
- Vaverka, J., Pellinen-Wannberg, A., Kero, J., Mann, I., De Spiegeleer, A., Hamrin, M., ... Pitkanen, T. (2017, August). Potential of Earth Orbiting Spacecraft Influenced by Meteoroid Hypervelocity Impacts. *IEEE Transactions on Plasma Science*, 45(8), 2048-2055. doi: 10.1109/TPS.2017.2676984
- Ye, S. Y., Gurnett, D. A., Kurth, W. S., Averkamp, T. F., Kempf, S., Hsu, H. W., ... Grün, E. (2014, August). Properties of dust particles near Saturn inferred from voltage pulses induced by dust impacts on Cassini spacecraft. *Journal of Geophysical Research (Space Physics)*, 119(8), 6294-6312. doi: 10.1002/2014JA020024
- Zaslavsky, A. (2015, February). Floating potential perturbations due to micrometeoroid impacts: Theory and application to S/WAVES data. *Journal of Geophysical Research (Space Physics)*, 120(2), 855-867. doi: 10.1002/2014JA020635
- Zaslavsky, A., Meyer-Vernet, N., Mann, I., Czechowski, A., Issautier, K., Le Chat, G., ... Kasper, J. C. (2012, May). Interplanetary dust detection by radio antennas: Mass calibration and fluxes measured by STEREO/WAVES. *Journal of Geophysical Research (Space Physics)*, 117(A5), A05102. doi: 10.1029/2011JA017480

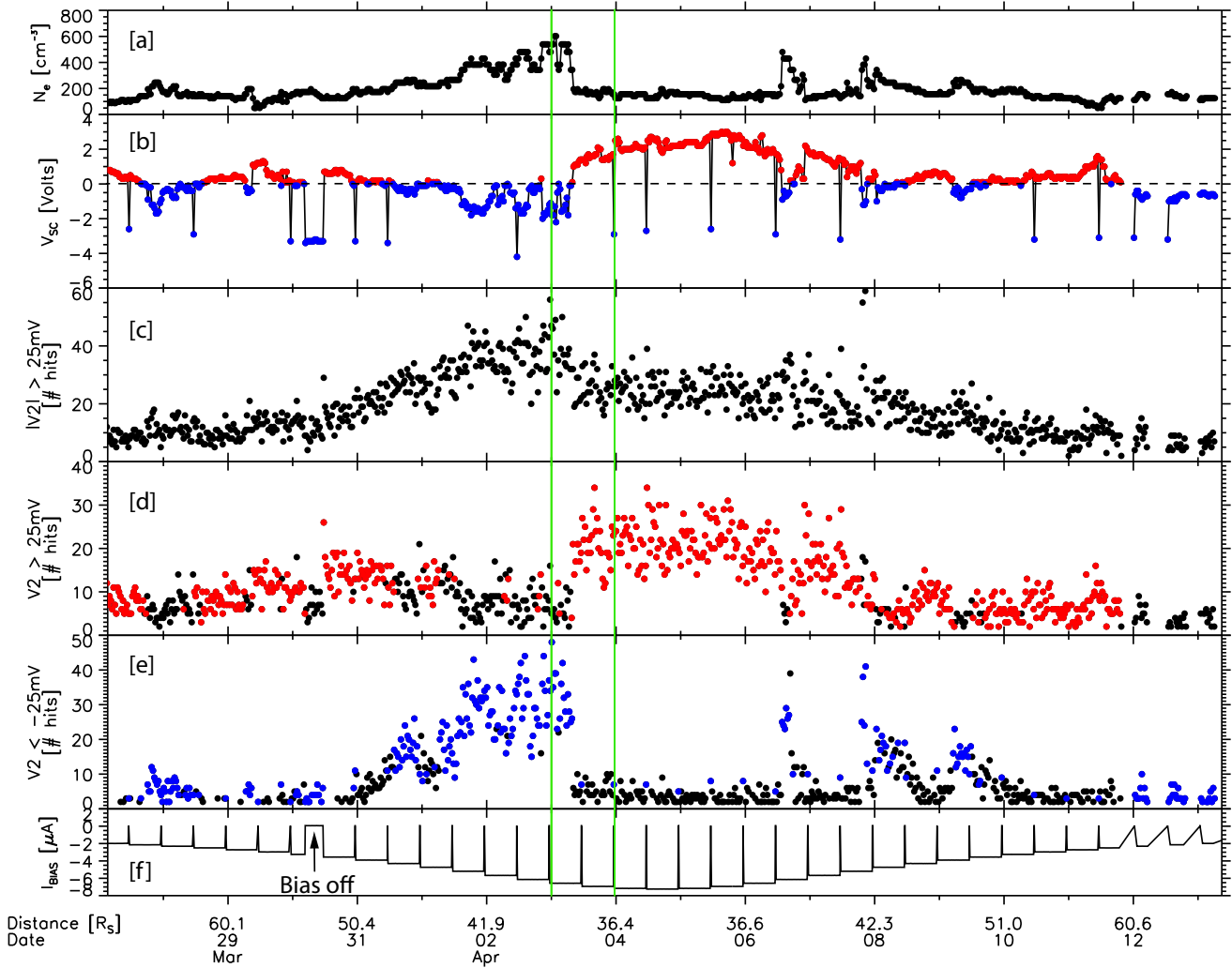


Figure 2. An overview of PSP Encounter 2 data, with perihelion at $35.7 R_S$ on April 5, 2019. Panel [a] is the total plasma density computed from the QTN spectrum. Panel [b] is the spacecraft potential proxy V_{SC} , colored for polarity (red > 0 , blue < 0). Panel [c] is the number of dust hits in 30 minute intervals estimated from $|V_2|$, showing an increase towards perihelion. Panel [d] is the number of dust hits in 30 minute intervals with positive polarity, where red dots are intervals of $V_{SC} > 0$. Panel [e] is the number of dust hits in 30 minute intervals with negative polarity, where blue dots are intervals of $V_{SC} \leq 0$. Panel [f] is the value of the applied bias current in μA . Spikey events are twice-daily bias sweeps, and an interval of no bias is indicated. Green vertical bars show the interval of April 3, 2019 with a large change of density and spacecraft potential/polarity. This figure shows clearly that intervals of negative (positive) V_{SC} correspond to clear enhancements in dust impulses with positive (negative) dominated TDS events; note that TDS measures $V_2 - V_G$, so that rapid voltage changes in V_G appear opposite polarity.

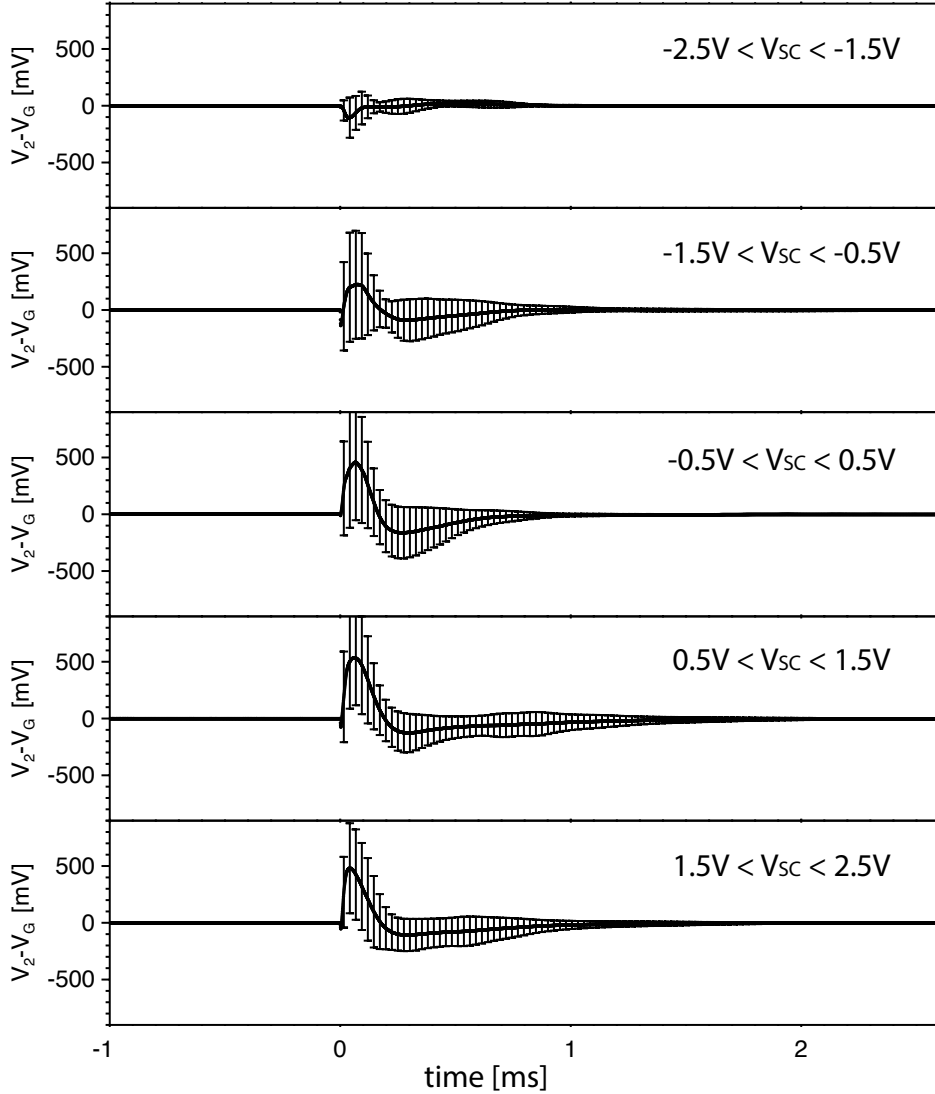


Figure 3. Superposed epoch plots of V2 monopole TDS waveform events, organized by spacecraft floating voltage V_{SC} . The black curve is the average waveform and error bars are one-sigma variations. The instrument saturates at $\approx \pm 1100$ mV. Table 1 collects the parameters associated with these intervals. Notably, the top panel with $V_{SC} < -1.5V$ shows that the typical waveform has its peak value with $V_2 - V_{SC} < 0$.

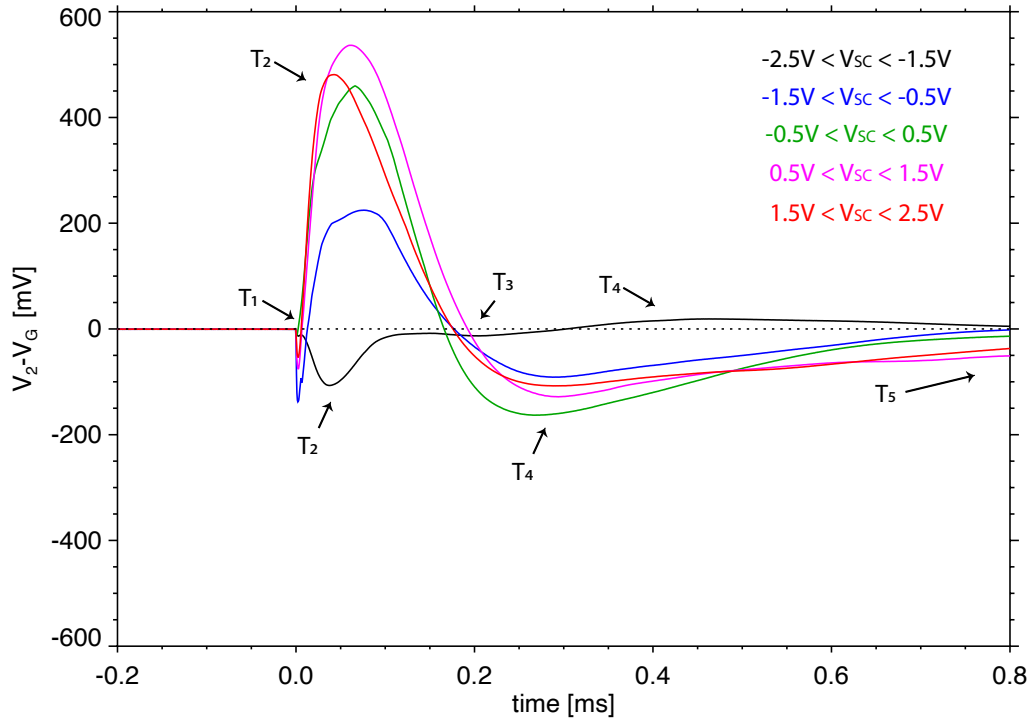


Figure 4. Epoch-averaged waveforms binned and colored by spacecraft potential. These are the average waveforms from Figure 3. Note that the waveform with $V_{SC} < -1.5V$ is opposite polarity to the others at both the primary peak at T_2 and the secondary peak at T_4 . Table 1 collects the waveform and plasma parameters.